

AD-A064 787

SCIENCE APPLICATIONS INC MCLEAN VA
TWO-DIMENSIONAL NUMERICAL MODEL OF THE NEAR-FIELD FLOW FOR AN O--ETC(U)
1977 G O ROBERTS, S A PIACSEK, J TOOMRE N00014-76-C-0610

F/G 20/4

UNCLASSIFIED

SAI-76-624-WA

NRL-GFD/OTEC-5-76

NL

OF
ADA
064787



END
DATE
FILMED

4 -79
DDC

18 NRL

19

NRL-GFD/OTEC-5-76

1 P.S.

UC-64

LEVEL

6

TWO-DIMENSIONAL NUMERICAL MODEL
OF THE NEAR-FIELD FLOW FOR AN OCEAN THERMAL POWER PLANT.
PART I. THE THEORETICAL APPROACH AND A LABORATORY SIMULATION.

ADA 064787

NOV 4 1977

11/19/77

Glyn O. Roberts

NRL# 533,030

2

Fluid Mechanics Division
Science Applications, Inc.

THE RUTH H. HOOKER
TECHNICAL LIBRARY

12 53p

JAN 17 1978

and

NAVAL RESEARCH LABORATORY

10

Glyn O. Roberts, Steve A. Piacsek and Juri Toomre

Geophysical Simulation Section, Code 7750
Naval Research Laboratory

DDC FILE COPY

DDC
REF ID: A64787
JAN 30 1979
REGISTERED
C Q

14

SAI-76-624-WA

Report written
in 1977

APPROVED FOR PUBLIC RELEASE
DISTRIBUTION UNLIMITED

15 71 0804-76-C-0610, E(49-26)-1005

Supported by the Ocean Thermal Energy Conversion Program,
Division of Solar Energy, Energy Research and Development
Administration, under ERDA contract E (49-26) 1005 .

408 404 79 01 18 045

JOB

Science Applications, Inc.
SAI-76-624-WA, Part I.
--Naval Research Laboratory,
NRL-GFD/OTEC 5-76.
TWO-DIMENSIONAL NUMERICAL MODEL OF
THE NEAR-FIELD FLOW FOR AN OCEAN
THERMAL POWER PLANT. Part I. THE
THEORETICAL APPROACH AND A LABORATORY
SIMULATION.
52 pgs., (Undated), 1977
Copy # (Rec'd) Date Copy # (Dest) Date
UNCLASSIFIED
1--12-16-77
2

NRL 533030

Roberts, G.O.
Placsek, S.A.
(NRL Author)
Toomre, J.
(NRL Author)

N00014-76-C-0610

TABLE OF CONTENTS

	<u>Page</u>
ABSTRACT.	3
1. INTRODUCTION.	4
2. EQUATIONS AND TURBULENCE MODEL.	7
3. THE OCEAN THERMAL POWER PLANT MODEL	14
4. BOUNDARY AND INITIAL CONDITIONS	17
5. NUMERICAL PROCEDURE FOR SOLVING THE EQUATIONS	22
6. A PROPOSED LABORATORY SIMULATION.	28
7. NUMERICAL RESULTS FOR THE PROPOSED EXPERIMENTAL SIMULATION.	33
ACKNOWLEDGMENTS	51
REFERENCES.	52

ACCESSION for	
NTIS	Write Section <input checked="" type="checkbox"/>
DDC	B.H. Section <input type="checkbox"/>
UNANNOUNCED	
DISSEMINATION	
BY	
DISTRIBUTION/AVAILABILITY CODES	
	SPECIAL
A	

79 01 18 045

ABSTRACT

↓ This report describes the computer model NRFLO2 which has been developed to calculate the near-field stratified turbulent flow driven by the intakes and outflows of an ocean thermal power plant. A two-dimensional geometry is assumed, with the power plant intakes and jet outflows modelled by boundary conditions on the left boundary of a rectangular domain. Horizontal flow through the right boundary, to or from the far-field, is allowed by assuming a pressure in hydrostatic equilibrium with the ambient density distribution. The code uses a first-order closure model to treat the stratified turbulence. Advanced numerical methods enable convergent and accurate solutions to be obtained rapidly and economically.

A simple laboratory simulation of two-dimensional stratified turbulence driven by intakes and jet outflows is proposed in order to address the general question of near-flow recirculation. Such an experiment would also provide vital data for verifying the code NRFLO2 and its successors, and for tuning the turbulence parameters to give the best agreement. Numerical results from NRFLO2 are presented for the proposed experimental simulation. They confirm our analysis predicting a stability limit on the far-field horizontal flow, and demonstrate the occurrence of recirculation for fast flow cases. ←

1. INTRODUCTION

Estimates of the resource availability and environmental impact of an ocean thermal power plant (OTPP) will require carefully designed computer models of the flows driven in the ocean waters immediately surrounding the plant. This report describes the computer model NRFLO2 developed to study the stratified turbulent motions resulting from the intakes and outflows of an OTPP. The application of NRFLO2 to particular OTPP engineering design configurations, such as discussed by Trimble (1975) and Douglass (1975), will be presented in subsequent reports.

An ocean thermal power plant operating in tropical waters uses warm surface water to boil a working fluid such as ammonia. The high pressure gas generates power by passing through a turbine, and is condensed at a low pressure using cold water from the deep ocean. A typical 200 MW power plant would take in 5×10^4 cu ft/sec of water from near the ocean surface, at about 80°F , and eject it at about 77°F . A similar volume flux would be removed from the deep ocean (at depth 1500 to 4000 ft) at about 40°F , and ejected at about 43°F after being used to condense the working fluid. Most designers envisage floating plants, though the early prototypes may be on land.

Our study of the turbulent external flow near an OTPP has two objectives. First, we wish to determine the average inflow temperatures, since their difference constitutes the thermal resource. For certain designs and ocean environments, there will be a substantial reduction in the average temperature of the warm inflow water, due to turbulent mixing and to recirculation of some of the outflow water from the plant. Our second objective is to obtain results from these near-field studies which can be used in calculating the far-field environmental impact of OTPP operation. A detailed discussion of the far-field effects and their background in geophysical fluid dynamics is given by Piacsek, Toomre, and Roberts (1975). Our calculations to be discussed here are confined to the

region near the plant, where the flows can deviate substantially from the horizontal, and the turbulence is very much stronger than in the ambient ocean. Far from the OTHF, the plant-induced addition to the ambient ocean currents is practically horizontal, and the plant-induced turbulence has decayed to negligible levels.

In this report, we describe a two-dimensional computer model NRFLO2, which we have used to obtain numerical results on the near-field flow. The differential equations are presented in Section 2, together with the first-order closure model used to represent the stratified turbulence. In our formulation, an extra equation is solved for the mean kinetic energy of the turbulent fluctuations. The single turbulent diffusivity is obtained from this in a novel way which serves to describe the physics of stratified turbulent transport and which does not allow the turbulence to decay to zero in a finite time. A further innovation aids in obtaining steady mean flows for strong stratification.

Our representation of the multiple inflows and outflows characteristic of an ocean thermal power plant is described in Section 3. The computational domain is rectangular, with the upper boundary representing the ocean surface. The left-hand boundary is occupied by the inlet and outlet ports of the OTHF. The finite computational domain is intended to represent a semi-finite portion of the ocean, and thus our other boundaries (lower and right-hand) must be suitably permeable and with an appropriate thermal stratification. The boundary conditions used to achieve this are described in Section 4, together with the initial conditions.

Section 5 provides a brief description of the numerical methods which we have employed in NRFLO2 in order to obtain accurate and convergent results. The code has been designed to be economical of machine time, despite the complexity of the problem. Implicit time-stepping is used to allow larger time steps as we evolve the solutions to a steady state. A non-uniform computational mesh is used to achieve good spatial resolution of the fairly complicated flow structures. Second-order accurate finite-differences are used throughout.

In Section 6, we propose and discuss a fairly simple laboratory experimental simulation of stratified turbulence driven by inflows and outflows, in support of our theoretical studies. The experiment is designed to investigate recirculation between the inlet and outlet ports, a matter of critical concern in this effort.

In the final Section 7, we present numerical results obtained by applying our code NRFLO2 to the proposed laboratory experimental simulation, for a range of flow rates. The results show that for low flow speeds, the inflow and outflow drive relatively independent fluid motions which are practically horizontal. Doubling the flow speed produces significant turbulent recirculation between the inflow and outflow ports, and doubling it again produces major recirculation. Such simplified experiments should play an important role in the design of actual OTHP prototypes.

2. EQUATIONS AND TURBULENCE MODEL

In this section, we present the equations used in our NRFL02 code to describe these stratified turbulent flows. The resulting equations (13) are listed at the end of the section, so that the discussion can be omitted on a first reading.

Using the usual Boussinesq approximation and a standard notation, the full equations of heat, momentum, and continuity are written as:

$$\partial_t T = \left\{ \kappa T_{,j} - u_j T \right\}_{,j} \quad , \quad (1a)$$

$$\partial_t u_i = b \delta_{i3} + \left\{ -P \delta_{ij} + \nu (u_{i,j} + u_{j,i}) - u_j u_i \right\}_{,j} \quad , \quad (1b)$$

$$u_{i,i} = 0 \quad . \quad (1c)$$

Here u_i is the velocity vector, T is temperature, and P is a modified pressure. Further, ν and κ are respectively the kinematic viscosity and the thermal diffusivity, and b is the upward buoyancy force $g \delta \rho / \rho$, taken as $g \alpha T$, where α , the coefficient at thermal expansion, is assumed constant. The third coordinate (x_3) is upwards, the usual summation convention is implied, and all spatial derivatives are indicated by the suffix notation, so that $u_{j,i}$ denotes $\partial u_j / \partial x_i$.

We will express the velocity field as:

$$u_i = \bar{u}_i + u_i' \quad ,$$

where \bar{u}_i is the average of an ensemble of flow realizations, and u_i' is a particular turbulent fluctuation from this average. The other variables like temperature will be written in the same form. Then taking the ensemble average of equations (1) yields:

$$\partial_t \bar{T} = \left\{ \kappa \bar{T}_{,j} - \bar{u}_j \bar{T} - \overline{u_j T'} \right\}_{,j} \quad , \quad (2a)$$

$$\partial_t \bar{u}_i = \bar{b} \delta_{i3} + \left\{ -\bar{p} \delta_{ij} + \nu (\bar{u}_{i,j} + \bar{u}_{j,i}) - \bar{u}_j \bar{u}_i - \overline{u_j u_i} \right\}_{,j} \quad , \quad (2b)$$

$$\bar{u}'_{i,i} = 0 \quad . \quad (2c)$$

Here, the long overbars denote ensemble averages of products of the turbulent fluctuations u'_i and T' . Thus, $-\overline{u_j T'}$ is the turbulent heat flux, and $-\overline{u_j u_i}$ is the Reynolds stress. Subtracting equations (2) from equations (1) yields the turbulent fluctuation equations,

$$\partial_t T' = \left\{ \kappa T'_{,j} - \bar{u}_j T' - u_j \bar{T} - (u_j T')' \right\}_{,j} \quad , \quad (3a)$$

$$\partial_t u'_i = b' \delta_{i3} + \left\{ -p' \delta_{ij} + \nu (u'_{i,j} + u'_{j,i}) - \bar{u}_j u'_i - \overline{u_j u_i} - (u'_j u'_i)' \right\}_{,j} \quad , \quad (3b)$$

$$u'_{i,i} = 0 \quad . \quad (3c)$$

It is not practicable to solve equations (1) or (3) for a very large number of flow realizations, in order to obtain the mean temperature distribution \bar{T} and the mean flow \bar{u}_i by averaging. Instead, statistical turbulence models (Piacsek, Toomre, and Roberts, 1975) are used to obtain equations for $\overline{u_i T'}$ and $\overline{u'_j u'_i}$ which are partly empirical, but are motivated by equations (3).

In zero-order turbulence modelling, the turbulent heat flux and the Reynolds stress are determined by the equations

$$-\overline{u_j T'} = (K - \kappa) \overline{T}_{,j} \quad , \quad (4a)$$

$$-\overline{u_j u_i'} = (K - \nu) (\overline{u_{i,j}} + \overline{u_{j,i}}) - \frac{2}{3} E \delta_{ij} \quad , \quad (4b)$$

where the turbulent diffusivity K is an imposed function of position, and E is the turbulent kinetic energy density $\frac{1}{2} \overline{u_i' u_i'}$. In general, K can be a tensor rather than a scalar, and can be different in equations (4a) and (4b).

In second-order statistical turbulence modelling, the quantities $\overline{u_i' T'}$ and $\overline{u_j' u_i'}$ obey partial differential equations, with time derivative terms, advection terms, generation terms, diffusion terms, and decay terms. These equations are as far as possible derived from equations (3), but are partly empirical, involving concepts such as the length scale or turnover time of the turbulence, as in the following discussion of first-order closure.

We adopted for the code NRFLO2 a first-order statistical closure model using equations (4), with K determined from an imposed length scale L and a turbulent kinetic energy equation. This equation is obtained by multiplying equation (3b) by u_i' , taking the ensemble average, and modelling certain terms. With

$$\overline{E} = \frac{1}{2} \overline{u_i' u_i'} \quad , \quad (5)$$

the resulting turbulent kinetic energy equation is

$$\begin{aligned} \partial_t \overline{E} &= \overline{u_3' b'} - \overline{u_{i,j}} \overline{u_i' u_j'} + \left\{ -\overline{u_j' (P' + E')} \right. \\ &\quad \left. + \nu \overline{u_i' (u_{i,j}' + u_{j,i}')} - \overline{u_j' E} \right\}_{,j} - \frac{\nu}{2} \overline{(u_{i,j}' + u_{j,i}')^2} \end{aligned} \quad (6)$$

The first two terms on the right of equation (6) represent, respectively, the loss of turbulent kinetic energy in creating mean potential energy, and the generation of turbulent kinetic energy from the shear of the mean flow. We write the buoyancy-related term $\overline{u_3 b}$ as $g\overline{u_3 T}$. Equations (4) can then be used to approximate these first two terms. The third term can be interpreted as the divergence of a flux of turbulent kinetic energy; the first two parts are modelled as

$$\left\{ -\overline{u_j'(P'+E')} + \overline{v u_i'(u_{i,j}' + u_{j,i}')}\right\}_{,j} = \left\{ \overline{KE}_{,j} \right\}_{,j} \quad (7)$$

The last term in equation (6) represents the loss of turbulent kinetic energy by a cascade through the spectrum to small length scales where it is dissipated by viscosity. This process occurs on a time scale proportional to the turnover time for the largest eddies, so that the last term is modelled as

$$-\frac{v}{2} \overline{(u_{i,j}' + u_{j,i}')^2} = -c_f \overline{E}/\tau \quad , \quad (8)$$

where c_f is a numerical coefficient and τ is a turnover time scale.

In unstratified turbulence with first-order modelling, usually $K = \overline{LE}^{1/2}$ and $\tau = \overline{LE}^{-1/2}$, where the length scale L is an imposed constant or function of position, or is determined from another empirical equation. When dealing with turbulence in a stratified medium, the importance of the stratification is measured by the dimensionless ratio $N^2 L^2 / \overline{E}$ where N^2 is $\overline{b}_{,3}$ and N is the Brunt-Vaisala frequency of internal waves. When this ratio is very small, the turbulent eddies turn over in a time short compared with $1/N$, and the stratification is negligible. When the ratio is very large, the random motions are more like internal waves than turbulent eddies and the system of equations (3) is effectively linear in the turbulent fluctuations.

This has two consequences. There is practically no nonlinear cascade of turbulent kinetic energy to small length scales where it is lost through viscous dissipation. Also, there is effectively no vertical diffusion of heat; a vertically displaced fluid element bounces back to its undisturbed elevation without mixing. When the dimensionless ratio N^2L/\bar{E} is of order unity, the random internal waves are sufficiently nonlinear to break at irregular intervals, resulting in some vertical diffusion and in some turbulent kinetic energy loss through the cascade.

The unstratified formulae $K = L\bar{E}^{-1/2}$ and $\tau = L\bar{E}^{-1/2}$ therefore give too large a diffusivity and too small a time scale for energy cascade, when stratification is important and the dimensionless ratio is of order unity or larger. In addition, when this K expression is used in modelling, the first term on the right-hand, the turbulent kinetic energy density \bar{E} , decays locally to zero in a finite time. For this reason, we have adopted for the code NRFLO2 the following expressions for K and τ ,

$$K = L\bar{E}^{-1/2}(1 + c_s N^2 L^2 / \bar{E})^{-1} \quad , \quad (9)$$

$$\tau = L^2 / K \quad , \quad (10)$$

with L an imposed constant length scale and c_s a constant.

For our modelling of the external flow for an OTTP, we have made further modifications to the system of equations (2) and (4) to (10) to give steady solutions when the dimensionless ratio N^2L^2/\bar{E} is large. The mean flow variables \bar{T} , \bar{u}_1 , and \bar{E} must be steady, from their definition as the average over an ensemble of flows maintained by steady boundary conditions. And in cases with reasonably strong mean flow and turbulence, we have obtained steady solutions by time-stepping the above equations. But in other cases, we obtained a finite amplitude

oscillation; it appears that the unmodified system of equations does have a steady solution, but this solution is unstable to small disturbances when the turbulent diffusivity K is small.

We have considered three ways of resolving this difficulty that the mean flow variables oscillate in time when the dimensionless ratio $N^2 L^2 / \bar{E}$ is small. The first is the rational approach of time averaging the oscillations, but such a procedure is of questionable accuracy. The second approach is to look for steady solutions to the same equations by a method which does not involve marching them forward in time, thus avoiding the instability. The third method is to modify the equations and the turbulence modelling in order to suppress the instability. This could be achieved by a large and totally artificial increase in the turbulent diffusivity K ; the results will then be steady, but numerically incorrect. A more subtle change in the equations is required, and it is this approach which we have implemented in our NRFLO2 code.

To achieve this, we have added the term

$$-(c_w KN^2 / \bar{E}) \bar{u}_3 \quad , \quad (11)$$

on the right-hand side of the \bar{u}_3 equation. The term taken alone would make \bar{u}_3 tend to zero on a time scale of $(c_w KN^2 / \bar{E})^{-1}$. When used in combination with the other terms, and with the consistent addition of the term

$$(c_w KN^2 / \bar{E}) \bar{u}_3^2 \quad , \quad (12)$$

to the right-hand side of the turbulent kinetic energy equation (6), it serves to suppress the fluctuating vertical motions associated with the instability of the mean flow, and to generate turbulent kinetic energy instead. With these added terms (11) and (12), we have been able to obtain steady mean flows for a wide range of OTHP flow simulations.

The resulting equations used in NRFLO2 are

$$\partial_t \bar{T} = \left\{ K\bar{T}_{,j} - \bar{u}_j \bar{T} \right\}_{,j} , \quad (13a)$$

$$\begin{aligned} \partial_t \bar{u}_i = & (g\alpha\bar{T} - c_w KN^2 \bar{u}_3 / \bar{E}) \delta_{i3} + \left\{ -\bar{P}_E \delta_{ij} \right. \\ & \left. + K(\bar{u}_{i,j} + \bar{u}_{j,i}) - \bar{u}_j \bar{u}_{i,j} \right\}_{,j} , \end{aligned} \quad (13b)$$

$$\bar{u}_{i,i} = 0 , \quad (13c)$$

$$\begin{aligned} \partial_t \bar{E} = & K \left\{ -N^2 + \frac{1}{2}(\bar{u}_{i,j} + \bar{u}_{j,i})^2 - c_f \bar{E} / L^2 \right. \\ & \left. + c_w N^2 \bar{u}_3^2 / \bar{E} \right\} + \left\{ K\bar{E}_{,j} - \bar{u}_j \bar{E} \right\}_{,j} , \end{aligned} \quad (13d)$$

$$N^2 = g\alpha\bar{T}_{,3} , \quad (13e)$$

$$K = \bar{L} \bar{E}^{1/2} / (1 + c_s N^2 L^2 / \bar{E}) , \quad (13f)$$

where \bar{P}_E is $\bar{P} + \frac{2}{3}\bar{E}$ in equation (13b), and a term $-\frac{1}{2}v(\bar{u}_{i,j} + \bar{u}_{j,i})^2$ has been dropped from equation (13d) on the assumption $v \ll K$.

Equations (13) involve four parameters, the length scale L and the dimensionless constants c_f , c_s and c_w . These must be determined by tuning their values so that the numerical solutions are in satisfactory agreement with the results of laboratory experiments. The thermal expansion coefficient α is taken as $1.3 \times 10^{-4} / ^\circ\text{F}$, the appropriate value for temperatures near 60°F .

3. THE OCEAN THERMAL POWER PLANT MODEL

In the code NRFLO2, the ocean thermal power plant and its inflows and outflows are modelled by boundary conditions on the left boundary of the rectangular domain - $D \leq z \leq 0$, $0 \leq x \leq \gamma D$. Note that in describing our two-dimensional application of equations (13) we use x as the horizontal coordinate and z as the vertical coordinate, in place of x_1 and x_3 , and u and w for u_1 and u_3 . None of the currently suggested plant designs (Dugger, 1975) are described exactly by such a two-dimensional model, but it does serve to evaluate their primary flow characteristics.

For each of four inflows and outflows, the code uses a center height z_k , a radius r_k , a signed flux amplitude a_k , an angle α_k above the horizontal plane, a turbulence constant E_k , and a temperature T_k , together with the function

$$f(x) = \begin{cases} (1-x^2)^2 & \text{for } |x| \leq 1 \\ 0 & \text{for } |x| > 1 \end{cases} \quad (14)$$

The value of \bar{u} on the left boundary at height z is

$$\bar{u}(z) = \sum_1^4 \frac{a_k}{r_k} f\left(\frac{z - z_k}{r_k}\right) \quad (15)$$

Thus \bar{u} is zero except close to one of the z_k values, and is negative when a_k is negative (a plant inflow) and positive when a_k is positive (a plant outflow). The function $f(x)$ has been chosen to make the boundary value of \bar{u} a smooth function of z ; replacement of $(1-x^2)^2$ by 1 in equation (14) may give a more faithful description of certain plant designs or experimental simulations. If fewer than four plant inflows and outflows are to be modelled, then some of the a_k values can be set to zero.

For a plant outflow, where fluid is entering the computational region, boundary values must be imposed for \bar{w} , \bar{T} , and \bar{E} . The values are

$$\bar{w}(z) = \bar{u} \tan \alpha_k, \quad (16a)$$

$$\bar{E}(z) = E_k a_k^2 r_k^{-2}, \quad (16b)$$

$$\bar{T}(z) = T_k. \quad (16c)$$

Occasionally, slightly more complicated formulae are used in NRFL02 to allow for the possibility of overlapping outflow regions.

Since the power plant uses warm surface water to vaporise a fixed flux of working fluid, the warm outflow temperature is lower than the mean warm inflow temperature by a fixed amount. Similarly, the cold water inflow is used to condense the working fluid, and its temperature is increased a fixed amount before it is pumped out as the cold outflow. The code therefore evaluates the mean temperature T_k for each plant inflow region (a_k negative),

$$T_k = \frac{\int \bar{T} u dz}{\int \bar{u} dz}, \quad (17)$$

and adds or subtracts a given temperature increment to determine the corresponding outflow temperature T_k . This is optional; the code can also use fixed T_k values for plant outflows as in the experimental simulation described in Section 6.

We point out here that the NRFL02 code has the flexibility to describe a variety of plant designs. Further, it can be used to evaluate a portion of a given design, to evaluate for example just the cold inflow, or just the warm inflow and the two outflows. This flexibility

in the code allows it to be used to describe other configurations, such as the heated outfall from a conventional power plant, or the simple experimental simulation presented in Sections 6 and 7.

4. BOUNDARY AND INITIAL CONDITIONS

In many hydrodynamic simulations, the boundary conditions of symmetry or periodicity are essentially passive, and are only minor aspects of the problem. In our near-field simulations for ocean thermal power plants, it is the boundary conditions on the left boundary, described in Section 3, which drive the flow, and the remaining boundary conditions which control it.

At large distances from an OTPP operating in a stratified ocean, the flow is essentially horizontal, and the outflow water from the near-field region has found its own density level. Thus a primary requirement for a numerical simulation of the near flow is a set of boundary conditions at the right-hand edge of a finite computational domain, which make this boundary permeable and allow horizontal inflow and outflow at the correct density levels.

A second requirement is that the boundary conditions where the flow is out of the computational region should be passive. They should not produce significant outflow boundary layers, nor should failure to resolve these boundary layers numerically lead to upstream influence.

A third desirable feature for these boundary conditions is that during time-stepping towards a steady solution of the equations, they should make the boundary permeable to internal waves, and not allow them to reflect. As stated in Section 2, there are difficulties in these computations over instability of the mean flow solution; a boundary condition which reflects oscillations will increase these difficulties.

In our code NRFL02, we assume the ambient ocean \bar{T} , \bar{w} , and \bar{E} distributions are

$$T_a(z) = T_t + T_r \tan^{-1}\left\{(z + d_t)/z_t\right\} \quad , \quad (18a)$$

$$w_a = 0 \quad , \quad (18b)$$

$$E_a(z) = E_0 \exp(z/z_E) \quad , \quad (18c)$$

where T_t is the thermocline temperature, T_r the thermocline temperature range, z_t the thermocline thickness, and d_t the thermocline depth, while the turbulent kinetic energy density amplitude and depth scale are E_0 and z_E respectively.

Equation (18a) implies a temperature variation from $T_t - \pi T_r/2$ at great depths to $T_t + \pi T_r/2$ at large z (though z is of course confined to negative values). Parameter values can be chosen so that this profile is a satisfactory approximation to most real temperature profiles. According to equation (13e), the corresponding Vaisala frequency N of internal gravity waves in the undisturbed ocean is given by

$$N^2 = g\alpha T_r z_t \left\{ z_t^2 + (z + d_t)^2 \right\}^{-1} \quad . \quad (19)$$

Equation (18c) is a reasonable choice, since the ambient turbulence in the upper layers of the ocean is mostly due to the wind-driven surface waves, and decreases with depth. In fact, the rate of decrease is more rapid when N^2 is large. But since the ambient turbulence is much smaller than the turbulence produced by the plant, our solutions are relatively insensitive to E_0 and z_E , and thus equation (18c) is adequate.

At the ocean surface $z = 0$ and at the lower boundary of the computational domain $z = -D$, we apply the boundary conditions

$$\bar{w} = 0 \quad , \quad (19a)$$

$$\bar{u}_{,z} = 0 \quad , \quad (19b)$$

$$\bar{T}_{,z} = 0 \quad , \quad (19c)$$

$$\bar{E}_{,z} = 0 \quad , \quad (19d)$$

where $\bar{u}_{,z}$ denotes $\partial \bar{u} / \partial z$.

Thus there is zero normal flow, and zero turbulent flux of horizontal momentum, heat, and turbulent kinetic energy across these boundaries. In applying equations (19b), (19c) and (19d) at the surface, we are neglecting respectively the momentum flux across the surface produced by wind stress, the heat flux (due to solar heating, sensible heat transfer, and evaporative and radiative cooling), and the generation of a flux of turbulence at the surface by wind and waves. Each approximation is justified by the fact that the order of magnitude of each of these fluxes in our near-field computation is much larger than the geophysical surface fluxes.

We next describe our boundary conditions at the left and right boundaries of the computational domain. On the left boundary, the normal velocity \bar{u} is given by equation (15), representing the OTPP inflows and outflows. In order to satisfy our first requirement that the right boundary be permeable, allowing horizontal inflow and outflow with the appropriate temperature for each depth, we have applied the equation

$$\bar{P}_{E,z} = g\alpha T_a \quad , \quad (20)$$

at $x = \gamma D$, where T_a is the ambient temperature distribution (18a). This implies a pressure distribution in hydrostatic balance with the buoyancy force associated with the ambient temperature distribution. From equation (13b), this balance must apply at large distances from the plant, when the flow is horizontal and the turbulent kinetic energy density and the turbulent diffusivity are negligibly small. With the boundary condition (20), the only possible horizontal flow solution near the boundary $x = \gamma D$ must have the mean temperature distribution $\bar{T}(x,z) = T_a(z)$.

We further need boundary conditions on \bar{T} , \bar{w} , and \bar{E} at the side boundaries. These boundary conditions take a different form

depending on whether the horizontal flow is into or out of the computational domain. For outward flow, the boundary conditions must be passive, to satisfy our requirement that no significant outflow boundary layer be formed. For both outward and zero normal flow, we impose zero normal derivative on both vertical boundaries. Thus for \bar{u} not inward,

$$\bar{T}_{,x} = 0 \quad , \quad (21a)$$

$$\bar{w}_{,x} = 0 \quad , \quad (21b)$$

$$\bar{E}_{,x} = 0 \quad , \quad (21c)$$

on $x = 0$ and $x = \gamma D$. For inward flow, the values of \bar{T} , \bar{w} , and \bar{E} are determined by equations (16) for the left boundary (the OTPP outflow values), and by equations (18) for the right boundary (the ambient ocean values).

Our third requirement, that the right boundary be permeable to internal waves, is not met by equation (20) and the other boundary conditions on the right. We have therefore added the further term

$$-\sigma(x,z)\bar{w} \quad (22a)$$

to the \bar{w} equation. Here σ is only non-zero close to the right hand boundary, where it serves to damp vertical motions. Incoming internal waves are absorbed by this "porosity" distribution (Piacsek and Roberts, 1975). For σ , we have used the equation

$$\sigma(x,z) = \frac{1}{2}N \left\{ 8(x/\gamma D - 1) \right\} \quad , \quad (22b)$$

where

$$g(\xi) = \exp \left\{ -\sinh(\sinh \xi) \right\} \quad . \quad (22c)$$

The initial conditions for equations (13) can be stated readily. The NRFLO2 calculations are initiated by asserting ambient ocean conditions (18) throughout the computational domain. Further, the initial horizontal velocity profile at all values of x is the same function of z as that prescribed on the left boundary by equation (15). We have chosen these initial conditions, with horizontal flow and very weak turbulence, so that any recirculation which occurs is not due to the initial conditions. In fact, our calculations have not provided evidence for any hysteresis effects of the initial conditions on the final steady solution.

5. NUMERICAL PROCEDURE FOR SOLVING THE EQUATIONS

In this section we give a brief summary of the numerical methods we have used to solve equations (13), with the initial and boundary conditions described in Sections 3 and 4. Since prolonged calculations are envisaged for a large number of flow situations and for different parameter ranges, the numerical procedures must be very efficient. Further, it is desirable that the computer code used to implement these methods should possess a structure with a high degree of clarity and flexibility.

We begin by describing the non-uniform computational mesh used in our finite-difference representation of the equations. We use a small mesh spacing only near the left boundary and near the plant inflows and outflows, where it is needed to resolve the small length scales present. Elsewhere we use a larger mesh interval, to economize on mesh points. The mesh spacing varies smoothly.

Our computational mesh is staggered, as shown in Figure 1, for greater efficiency in representing equations (13). The variables \bar{T} , \bar{E} , \bar{P}_E and K are defined at the mesh points (x_m, z_n) for integer values of m and n , while \bar{u} is defined for integer n and half-odd m , and \bar{w} for integer m and half-odd n . It has long been known that this mesh is much more convenient and accurate for calculations involving the primitive variables. Most of the required first derivatives can be represented using neighboring mesh points, thus $\bar{u}_{,x} + \bar{w}_{,z}$ in equation (13c) is conveniently represented at the \bar{T} points, and $\bar{P}_{E,x}$ and $\bar{P}_{E,z}$ are conveniently represented at the \bar{u} and \bar{w} points.

Our boundaries are placed between the mesh lines, rather than on them, in representing the boundary conditions. As shown in Figure 1, the side boundaries are at $x_{1\frac{1}{2}}$ and $x_{M-\frac{1}{2}}$, and the bottom and surface boundaries are at $z_{1\frac{1}{2}}$ and $z_{N-\frac{1}{2}}$. This choice puts the normal velocity components on the boundary, and makes for high accuracy in representing the normal derivatives of the other variables.

Next we describe the numerical representation used for the

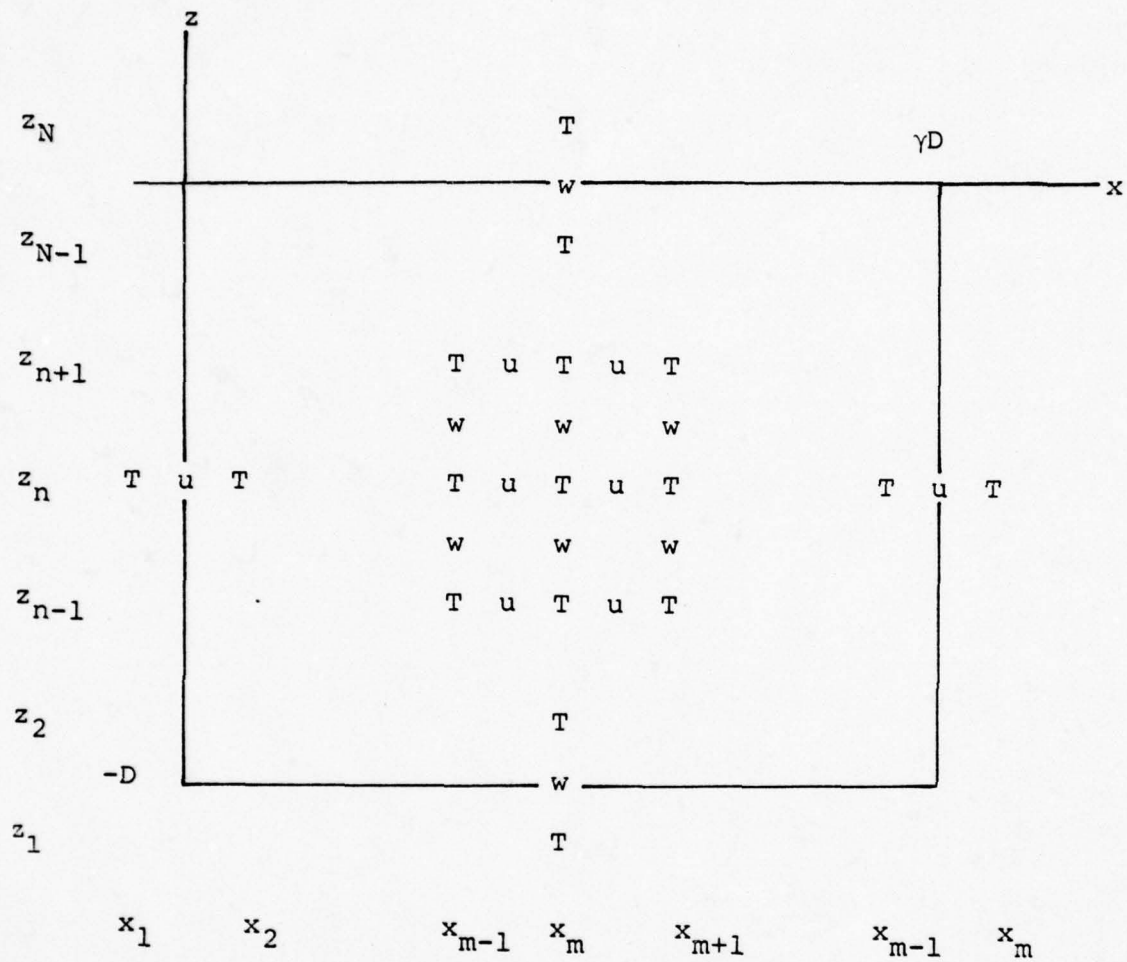


Figure 1. The non-uniform staggered computational mesh. \bar{T} , \bar{E} , \bar{P}_E and K are represented by their values at the T points, while \bar{u} and \bar{w} are represented by their values at the staggered mesh points indicated. The boundaries are at $x_{1\frac{1}{2}}$, $x_{m-\frac{1}{2}}$, $z_{1\frac{1}{2}}$, $z_{n-\frac{1}{2}}$. This leads to greater accuracy, convenience, and efficiency in representing the equations and boundary conditions.

spatial derivatives in equations (13). For every term but one, we employ the simplest second-order accurate central difference representation available, with averaging from the neighboring two or four mesh points as required. The resulting finite difference equations conserve the volume flux, heat, and momentum, as implied by equations (13). The one deviation from central differences is the use of upwind differencing in representing the advection term in the turbulent kinetic energy equations (13d). For this term

$$(\bar{u}_j \bar{E})_{,j} = \bar{u} \bar{E}_{,x} + \bar{w} \bar{E}_{,z} \quad , \quad (23)$$

we use the representation

$$\begin{aligned} (\bar{u} \bar{E})_{,x} \Big|_m &= \frac{1}{2} (\bar{u} + |\bar{u}|) (\bar{E}_m - \bar{E}_{m-1}) / \delta x_{m-\frac{1}{2}} \\ &+ -(\bar{u} - |\bar{u}|) (\bar{E}_{m+1} - \bar{E}_m) / \delta x_{m+\frac{1}{2}} \end{aligned} \quad (24)$$

where the suffix n for the z mesh is understood and \bar{u} denotes $\frac{1}{2} (\bar{u}_{m-\frac{1}{2}} + \bar{u}_{m+\frac{1}{2}})$. This representation is only first-order accurate; it has been adopted to avoid negative \bar{E} values where there is flow from a region of small \bar{E} to a region of large \bar{E} and the intervening layer, which can be very thin, is not sufficiently resolved.

The boundary conditions described in Sections 3 and 4 are similarly represented using the simplest central difference method, with one exception. Where the flow is out of the computational domain (to the left or the right), the \bar{T} , \bar{w} and \bar{E} equations allow an outflow boundary layer of thickness $K/|\bar{u}|$. When this is smaller than $\delta x/4$, our resolution is inadequate, and there is a tendency for mesh separation, with the variables at even mesh points separating from the variables at odd mesh points. This tendency is eliminated, and results of greater accuracy are obtained, by replacing the boundary condition of zero first derivative with zero second normal derivative, even when the representation is only first order.

We have chosen to represent the time evolution of equations (13) with second order accuracy, in spite of the fact that we are mainly concerned with time-stepping to a steady solution. Due to the extreme nonlinearity of the equations and our desire to avoid the artificial instability or dissipation associated with other explicit representations, we were forced to use a "leapfrog" method for time-stepping equations (13). The diffusion terms were treated by an alternating direction implicit method. We write the equations (13a,b,d) as:

$$\partial_t f = Q + Xf + Zf \quad , \quad (25)$$

where f can be \bar{T} , \bar{u} , \bar{w} , or \bar{E} ;

X and Z are the diffusion terms involving two differentiations with respect to x and z ;

Q represents the rest of the terms in the equation.

Then for time $k\delta t$, where k is an integer, our representation of equation (25) is

$$(f^* - f^{k-1})/\delta t = Q^k + X^k f^{k-1} + Z^k f^* \quad , \quad (26a)$$

$$(f^{k+1} - f^*)/\delta t = Q^k + X^k f^{k+1} + Z^k f^* \quad . \quad (26b)$$

At the beginning of the time step all quantities f^{k-1} and f^k are known, and thus Q^k can be evaluated. The z -diffusion is done implicitly in the first stage, and the x -diffusion in the second. The intermediate quantity f^* is a second-order approximation to f^k .

Equations (26) are subject to the well-known leapfrog instability when applied to the turbulent kinetic energy density equation (13d), because the N^2 and $c_f \bar{E}/L^2$ terms in the first bracket are decay terms. To avoid this instability, in which \bar{E}^k for even k separates from \bar{E}^k for odd k , we subtract the term $2a^k(\bar{E}^* - \bar{E}^k)$ from the right hand side of equation (26a), and the corresponding term $a^k(\bar{E}^{k+1} - 2\bar{E}^k + \bar{E}^{k-1})$ from the right hand side of equation (26b).

Here

$$2a^{k+} \left\{ -N^2 + \frac{1}{2}(\bar{u}_{i,j} + \bar{u}_{j,i})^2 - c_f \bar{E}/L^2 + c_w N^2 \bar{w}^2 / \bar{E} \right\} \partial K / \partial \bar{E} \\ -K(c_f/L^2 + c_w N^2 \bar{w}^2 / \bar{E}^2) > 0 \quad . \quad (27)$$

A suitable a^k expression is evaluated and applied in the code.

The pressure \bar{P}_E^k remains to be determined, in order to apply equations (26) to equation (13b). We write

$$\bar{P}_E^k = P_1^k + P_2^k \quad , \quad (28)$$

where P_1^k is obtained by extrapolation from previous values,

$$P_1^k = 2\bar{P}_E^{k-1} - \bar{P}_E^{k-2} \quad , \quad (29)$$

so that P_2^k remains unknown, but is of order δt^2 . Then P_1^k is used in evaluating Q in equation (25), and equations (26) determine \bar{u}_2 and \bar{w}_2 which are third order approximations to \bar{u}^{k+1} and \bar{w}^{k+1} , and do not satisfy equation (13c). We then add the effects of $P_{2,x}^k$ and $P_{2,z}^k$, applied for a time interval $2\delta t$,

$$(\bar{u}^{k+1} - \bar{u}_2)/2\delta t = -P_{2,x}^k \quad , \quad (30a)$$

$$(\bar{w}^{k+1} - \bar{w}_2)/2\delta t = -P_{2,z}^k \quad . \quad (30b)$$

Taking the divergence and using equation (13c) gives

$$\nabla^2 P_2^k = (\bar{u}_{2,x} + \bar{w}_{2,z})/2\delta t \quad . \quad (31)$$

This Poisson equation is solved by a generalized form of Wachspress alternating-direction implicit iteration (Varga, 1962, Roberts and Piacsek, 1975) using four iterations, while imposing the boundary conditions,

$$P_2^k = 0, \text{ on } x = \gamma D, \quad (32a)$$

$$\partial P_2^k / \partial n = 0, \text{ on the other boundaries.} \quad (32b)$$

The resulting P_2^k solution is substituted in equations (28) and (30) to determine \bar{P}_E^k [for application of equation (29)] and the new velocity components.

With the numerical method described by equations (26), our code is still subject to the stability requirement

$$(N + |\bar{u}|/\delta x + |\bar{w}|/\delta z)\delta t \leq 1 \quad (33)$$

Since δt is the same at every mesh point and time step, an estimate must be made at the beginning of the calculation of the maximum value of the bracket which is likely to be encountered. The code uses

$$\delta t = c(N_{\max} + u_{\max}/\delta x_{\min})^{-1}, \quad (34)$$

where N_{\max} and u_{\max} are the maxima of the ambient stratification (19) and the left boundary velocity (15) respectively, and c is an input constant.

Leapfrog time-stepping (26) is subject to a weak computational instability, with the values separating at even and odd time-steps, even in the absence of decay terms. These parasite solutions are avoided by re-initializing the calculation every few time-steps. For initialization, in terms of equation (26), any previous r^k is forgotten, and r^{k-1} is used to evaluate Q^k , X^k , and Z^k in order to obtain an approximate r_1^{k+1} , with second-order accuracy. Then a new calculation can be started off from r^{k-1} using

$$r^k = \frac{1}{2} (r^{k-1} + r_1^{k+1})$$

6. A PROPOSED LABORATORY SIMULATION

Our code NRFLO2 calculates the flow in a rectangular domain representing the near-flow region closest to an ocean thermal power plant, where the flow deviates from the horizontal and where the turbulence generated by the plant is important. The rectangular region has impermeable boundaries at the top and bottom. The horizontal velocity is given on the left, with the temperature, vertical velocity, and turbulent energy density also being imposed where this velocity is out of the plant and into the region. The passive boundary conditions on the right allow horizontal inflow from and outflow to a large fluid region with assumed temperature and turbulent kinetic energy profiles.

This code NRFLO2 has four parameters: the turbulence length scale L , and the three dimensionless parameters c_p , c_s , and c_w . Before the code can be used with any confidence to simulate the external flow of an ocean thermal power plant, we must tune the values of these parameters so that the numerical results are in satisfactory agreement with the results of laboratory experiments. Such experiments should be two-dimensional, and involve the simultaneous effects of density stratification and of turbulent jet inflows and outflows from the region. To our knowledge, suitable experiments have not yet been done, but two experimental programs recently funded by ERDA should begin to correct this deficiency.

We now suggest an experiment which meets these conditions and which would provide a laboratory examination of the possibility of near-flow recirculation of the outflow water in OTHF operation, as well as of the far-field environmental effect. In addition, this experiment would provide data for verifying and tuning our code NRFLO2 and its successors.

The proposed experimental configuration for this OTHF near-field simulation is outlined in Figure 2. A long rectangular tank is filled with water to a depth of 4 ft, with the temperature increasing linearly from 40°F at the bottom to 80°F at the surface. At the

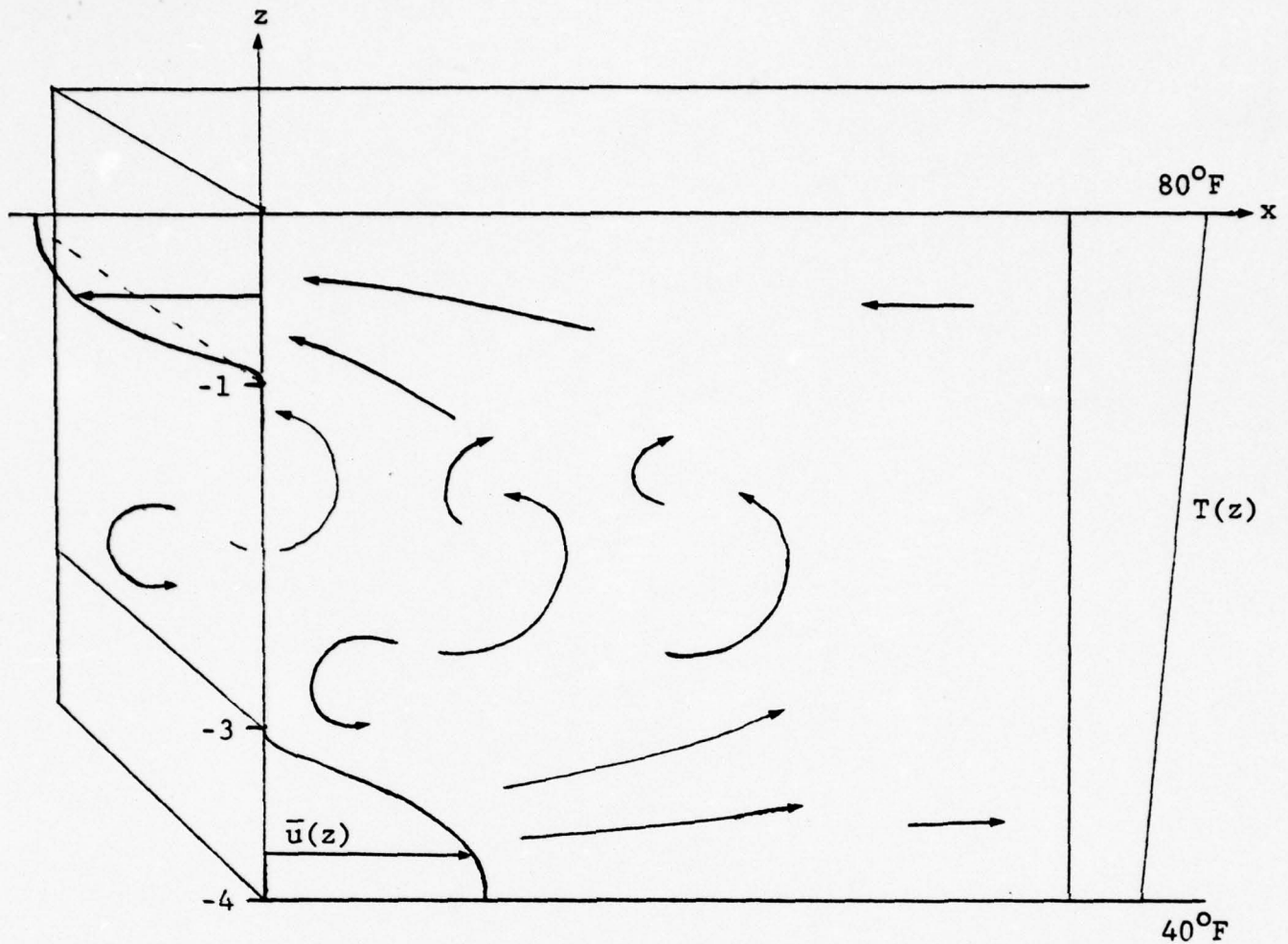


FIGURE 2

The proposed laboratory experiment configuration. A long tank is initially filled with water to a depth of 4 ft, with the temperature increasing linearly from 40°F at the bottom to 80°F at the free surface. Water at 40°F is pumped steadily in through the bottom gate on the left wall, and an equal volume flux is removed at the top. The inflow drives the indicated turbulent jet, entraining water from above. Further along the tank (beyond about 8 ft) the turbulence becomes very weak, and the flow is essentially horizontal, as indicated. The outflow from the tank comes partly from this far-field horizontal motion, and partly from the cold inflow; the mean outflow temperature can, therefore, range from almost 80°F for very slow flow to 40°F for very fast flow. The inflow and outflow maximum speeds $U = 2.68$ ft/sec, 1.34 ft/sec, and 0.67 ft/sec are studied numerically in Section 7.

beginning of the experiment the water is at rest. Cold water at 40°F is then pumped in steadily at the end of the tank, through a gate 1 ft high at the bottom, and taking up the full width of the tank. This flow simulates an OTPP outflow. To simulate a plant inflow, the same volume flux of water is simultaneously removed from the same end of the tank, through a similar gate extending 1 ft down from the surface. The maximum inflow speed U for the proposed experiment should be in the range from 0.2 ft/sec to 5 ft/sec. This speed range brackets the critical value described in the simple theoretical discussion of the resulting stratified turbulent flow provided in the remainder of this section.

In the absence of density stratification, a turbulent flow field is established fairly quickly in which all of the cold inflow water is sucked out again at the top of the tank. The mean flow and the turbulence intensity \bar{E} become very small at large distances (more than twice the depth) from the end of the tank. Thus, the far-field flow is zero.

With a density stratification, the situation is quite different. At large distances from the end of the tank, the turbulence is still very weak, but there can be substantial horizontal motion. This horizontal flow is established by very small horizontal density gradients, and is limited only by continuity (13c) and by the stability requirement,

$$N^2 \geq (\partial \bar{u} / \partial z)^2, \quad (35)$$

which follows from the first two terms in the turbulent kinetic energy density equation (13d). Physically, when this equation is satisfied, more turbulent energy is lost to creating potential energy than is gained from the shear. Thus, with N constant (from equation (13e)), N in these experiments is 0.204 sec⁻¹, the maximum stable far-field \bar{u} distribution is

$$\bar{u} = N(z + 2) (x/X - 1) \quad (36)$$

where X is the length of the tank, and the total flux $\int_{-4}^0 \bar{u} dz$ along the tank is zero. The continuity equation (13c) implies a very weak upwelling velocity, independent of x , and given by the equation

$$\bar{w} = -Nz(z + 4)/2X \quad , \quad (37)$$

for the maximum possible \bar{u} distribution (36). This upwelling, or the distribution corresponding to a \bar{u} smaller than (36), will eventually modify the ambient temperature distribution in the tank, in a time of order $1/\bar{w}$.

For small values of U , therefore, the cold inflow jet becomes a horizontal flow as the turbulence decays. The surface tank outflow simultaneously draws water steadily away from the surface layer. The resulting far-field flow is smaller than that given by equation (36), and is, therefore, stable. The average outflow temperature is almost 80°F , since all the outflow comes from near the surface and since minimal turbulent heat transfer occurs between the warm upper layers and the cold lower layers.

For larger U values, in a critical range and above, the far-field flow will be approximately given by equation (36). However, this flow is too small to carry away the cold inflow and to provide the water for the surface outflow. The remainder of the cold inflow water is sucked up and out with the surface outflow. (If carried over to an OTP design, this would imply recirculation of the cold plant outflow into the warm surface intake.) The average surface outflow temperature (17) decreases to 40°F as U becomes increasingly large, and the far-field warm surface water flow, with \bar{u} negative according to equation (36), is diluted with an increasing flux of cold inflow water.

According to equation (36), the maximum possible far-field outward cold flux $\int_{-4}^{-2} \bar{u} dz$ is $2N$, for $x \ll X$. Now the cold inflow flux $\int_{-4}^{-3} \bar{u} dz$ is λU , where U is the maximum speed and λ depends on the inflow profile, with $\frac{1}{2} < \lambda < 1$. So the critical U value, for which all the cold inflow can flow out to infinity, is $2N/\lambda$. This is about 0.77 ft/sec for the value $\lambda = 8/15$ used in Section 7.

For the laboratory experiment, the tank width should be at least 4 ft, to reduce three-dimensional effects on the mean flow. The length X should be at least 40 ft, to allow a reasonable period (about $3x/2$ sec) for establishment of a statistically steady turbulent flow before the upwelling (37) significantly modifies the temperature and density stratification. The temperature and the velocity components should be recorded, as functions of time, at a number of points in the flow, in order to evaluate the ensemble average (or time average) quantities \bar{T} , \bar{u} , \bar{w} , $\overline{u'T'}$, $\overline{w'T'}$, $\overline{u'u'}$, $\overline{u'w'}$, and $\overline{w'w'}$. The measurement points should be mainly in the first 8 ft, but should include a few points further along the tank to confirm our predictions of horizontal flow and small turbulent fluctuations. Most of the measurement points should be in the x - z plane at the center of the tank, to reduce effects of the sidewalls. These sidewall effects can be estimated by adding measurement points across the whole width of the tank at selected values of x and z .

7. NUMERICAL RESULTS FOR THE PROPOSED
EXPERIMENTAL SIMULATION

We have applied our code NRFL02 to the proposed experimental simulation of stratified turbulence driven by fluid jets and sinks, as described in Section 6. This numerical simulation of a proposed experiment has served three purposes. First, it has provided a simple and economical problem for code development, and for improving and optimizing the numerical methods of Section 5, since adequate resolution and convergence can be obtained with very few mesh points (about 12×12) and time-steps (about 100). Secondly, the numerical simulation has enabled us to study the effects of varying the dimensionless parameters c_f , c_s , and c_w , and the ratio of the turbulence length scale L to the given dimensions. Such studies will be of great value in tuning these parameters to give results agreeing with observations. Thirdly, the numerical results have demonstrated the existence of the far-field flow maximum (36) and the corresponding critical speed U for inflow to the experimental tank. This critical speed corresponds to an upper limit for the outflow of an ocean thermal power plant prototype, to avoid recirculation problems and thermal efficiency loss.

For our NRFL02 simulation of the proposed experiment, we took the horizontal flow \bar{u} on the left boundary $x=0$ as

$$\bar{u} = U \left\{ f(z + 4) - f(z) \right\} , \quad (38)$$

in conformity with equations (14) and (15). Thus, the inlet and outlet fluxes are $\lambda U \text{ ft}^2/\text{sec}$, where λ is $8/15$. In this report, we present numerical results for three different U values, 2.71 ft/sec, 1.35 ft/sec, and 0.68 ft/sec, which we designate respectively as strong flow, medium flow, and weak flow. These flow speeds, differing by factors of 2, have been chosen to examine conditions under which inflow and outflow recirculation may arise.

The portion of the left boundary, $x=0$, where \bar{u} is positive requires boundary conditions specifying \bar{w} , \bar{E} , and \bar{T} . In conformity with equations (16), we applied the boundary conditions

$$\bar{w} = 0 \quad , \quad (39a)$$

$$\bar{E} = U^2/5 \quad , \quad (39b)$$

$$\bar{T} = 40 \quad , \quad (39c)$$

for $-4 \leq z \leq -3$. We took the horizontal domain as $0 \leq x \leq 8$ ft for the simulations reported here; the use of larger values of x did not significantly change the results. Our choice of the four parameters L , c_f , c_s , and c_w for these numerical simulations was based on previous experience in the simulation of turbulent submarine wakes in a stratified ocean (Roberts and Piacsek, 1975; Warn-Varnas and Piacsek, 1976), together with a certain amount of testing. We adopted the following values

$$L = 0.4 \text{ ft.} \quad , \quad (40a)$$

$$c_f = 0.5 \quad , \quad (40b)$$

$$c_s = 0.1 \quad , \quad (40c)$$

$$c_w = 0.1 \quad . \quad (40d)$$

For the "ambient ocean" in equations (18), we took T_t as 60, d_t as 2, T_r and z_t very large, T_r/z_t as 10, E_o as $6.7 \times 10^{-6} \text{ ft}^2/\text{sec}^2$, and z_E as 2. These input parameters give the required uniform ambient temperature gradient and an E_a sufficiently small to be innocuous.

A major difference between the numerical simulation and the proposed experiment is in the bottom boundary condition (19b) that the normal derivative of \bar{u} is zero. In the experiment, \bar{u} vanishes at the bottom no-slip boundary. This difficulty can be overcome by using an inflow to the tank which is not at the bottom, and by modifying NRFL02 so that the boundary condition (19b) can optionally be replaced by zero \bar{u} .

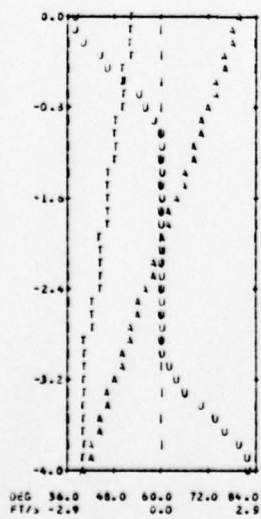
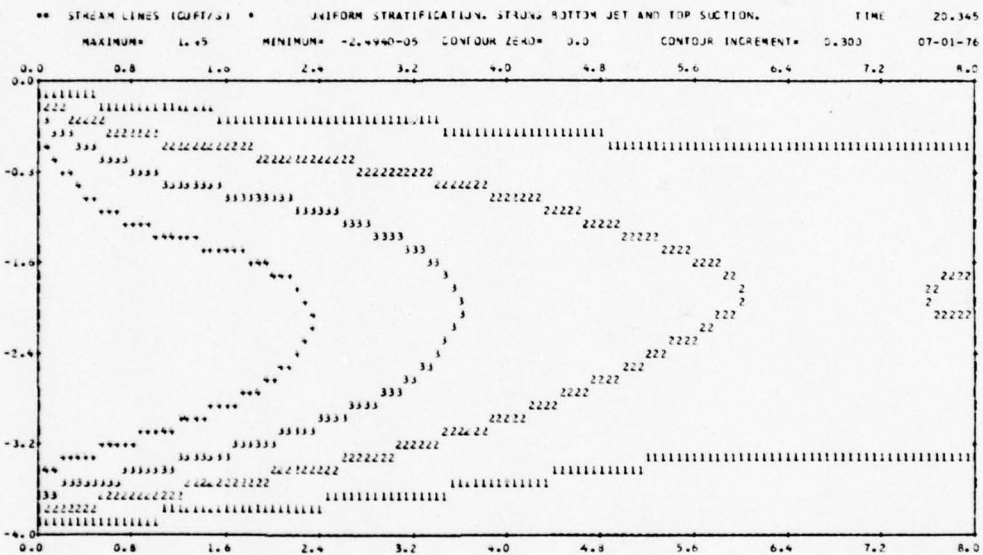
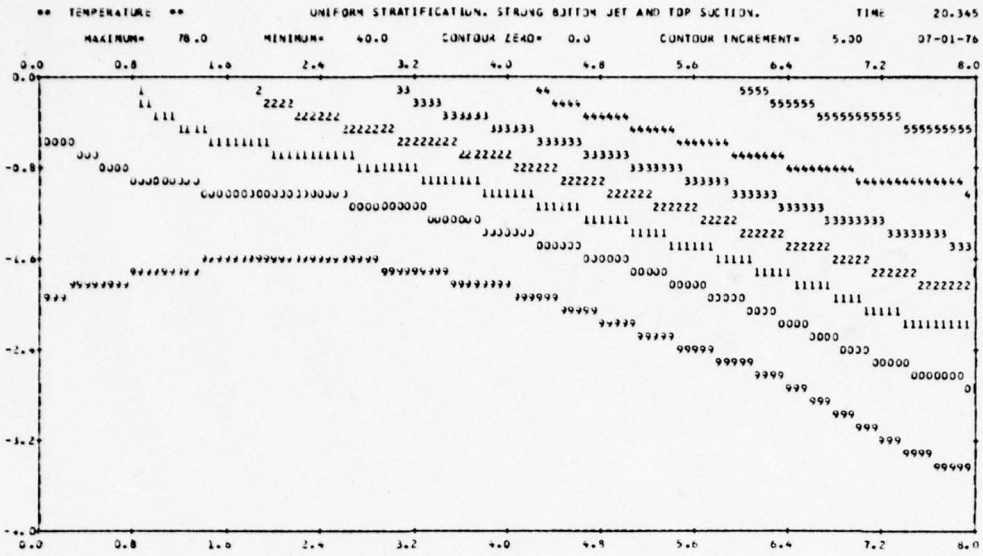
The numerical results for the three flow cases are displayed in Figures 3 to 8, which are photographic reproductions of the computer printout. Figures 3 and 4 are for the case designated as strong flow, Figures 5 and 6 are for the medium flow case, and Figures 7 and 8 are for weak flow. The format is the same for each pair of figures. In addition, Table 1 provides a summary of significant numerical values, for comparison purposes.

The upper panel of Figures 3, 5, and 7 shows the mean temperature solution $\bar{T}(x,z)$, for the three inflow speeds. The contour increment is 5°F in each case, so the curves labeled 9, 0, 1, 2, 3, 4, and 5 represent Fahrenheit temperatures of 45, 50, 55, 60, 65, 70, and 75. For strong flow (Figure 3) almost half the region is between 40°F and 45°F , while for weak flow (Figure 7) the temperature distribution is only slightly disturbed from the ambient uniform stratification.

The center panel of Figures 3, 5, and 7 is a contour plot of the streamlines of the mean flow, for the three cases. The units are ft^2/sec , or ft^3/sec per foot of tank width. The mean flow components \bar{u} and \bar{w} are $\psi_{,z}$ and $-\psi_{,x}$, where ψ is the stream-function. The contour increment is 0.3, 0.15, and $0.1 \text{ ft}^2/\text{sec}$ in the three cases, and the corresponding total influx and efflux at the left-hand side ($8U/15$) is 1.44, 0.72, and $0.36 \text{ ft}^2/\text{sec}$. Comparison of the three figures indicates that for strong flow most of the cold influx at the bottom left recirculates out at the top left (Figure 3), while for medium flow (Figure 5) only a small part of the mean flow recirculates. For weak flow (Figure 7) the stratification stops all recirculation, and the single streamline loop from the right boundary shows the effect of turbulent entrainment by the bottom jet.

FIGURE 3. Strong Flow Results

The center panel shows that most of the cold inflow at the bottom left recirculates along the streamlines and out at the top left. Only one streamline extends to the right boundary. In the upper panel, the temperature is not constant on streamlines because of turbulent mixing. The warm flux from the upper right shares its heat with the cold recirculating flux from the lower left. Further results are shown in Figure 4.



UNIFORM STRATIFICATION, STRONG BOTTOM JET AND TOP SUCTION.
 4 FOOT DEPTH EXPERIMENT SIMULATION. 1 FOOT JET AND SUCTION.
 BOTTOM JET TEMPERATURE IS 40 DEGREES FAHRENHEIT.
 TEMPERATURE RANGE 40 TO 80 DEGREES AT INFINITY.

AMP1	0.8000	-0.4000	0.0	0.0
AMP2	0.2000	0.2000	0.0	0.0
TAN1LF	0.0	0.0	0.0	0.0
TPA1K	40.0	0.0	0.0	0.0
RPL	0.250	0.250	0.000	2.000
ZCUT	0.0	1.000	0.0	0.0
TI,TI,ZTC,WID	80.0	40.0	0.700	1000.000
JAM3,QJEP	1.00-05	0.50		
TELE,CF,CH,PORC	0.100	0.500	0.100	0.500
SSP,STFAC,STRCH,II,JJ	2.000	1.000	3.0	12 12
TIME=CL,NOUTPT,OSCALE,WIDFT	30.0	0.80	2	4.0 1.0

MEAN PLANT INFLOW TEMPERATURE IS 49.8

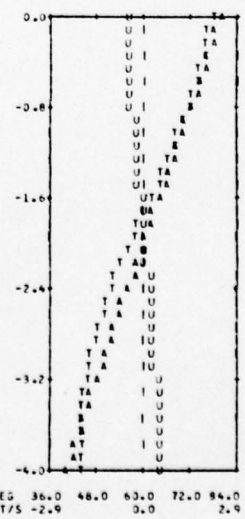
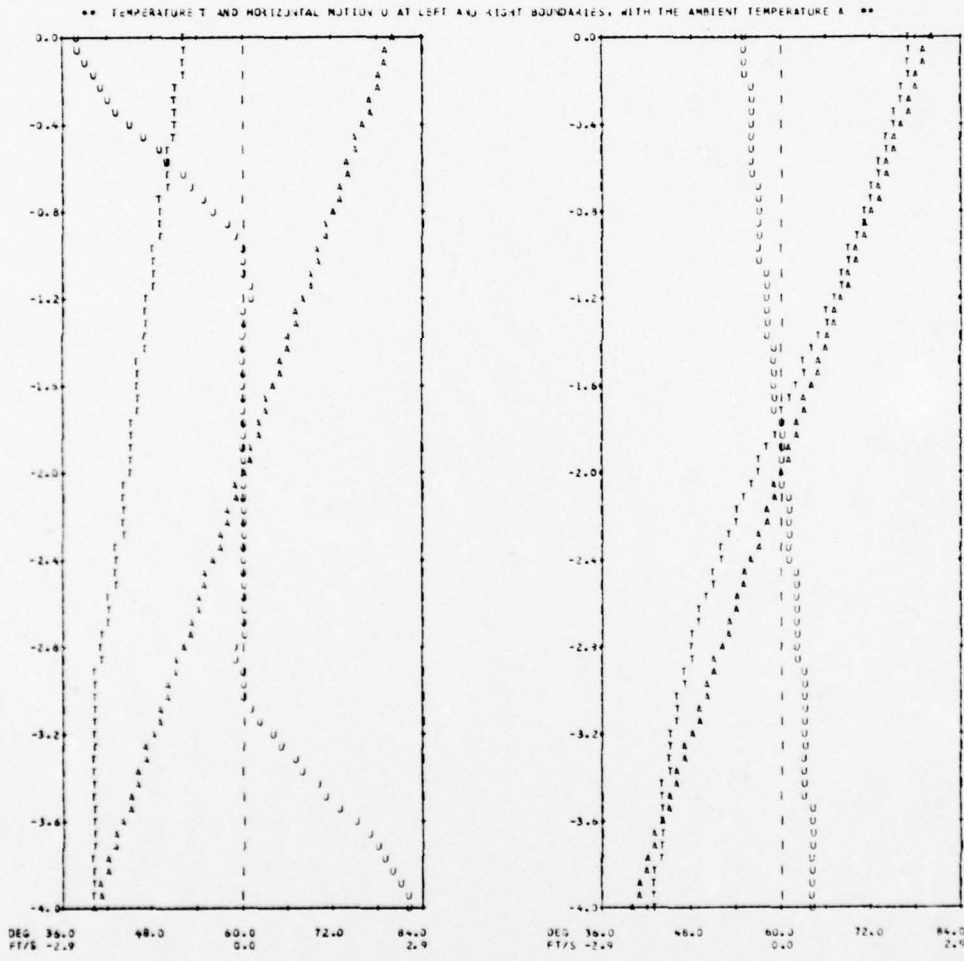
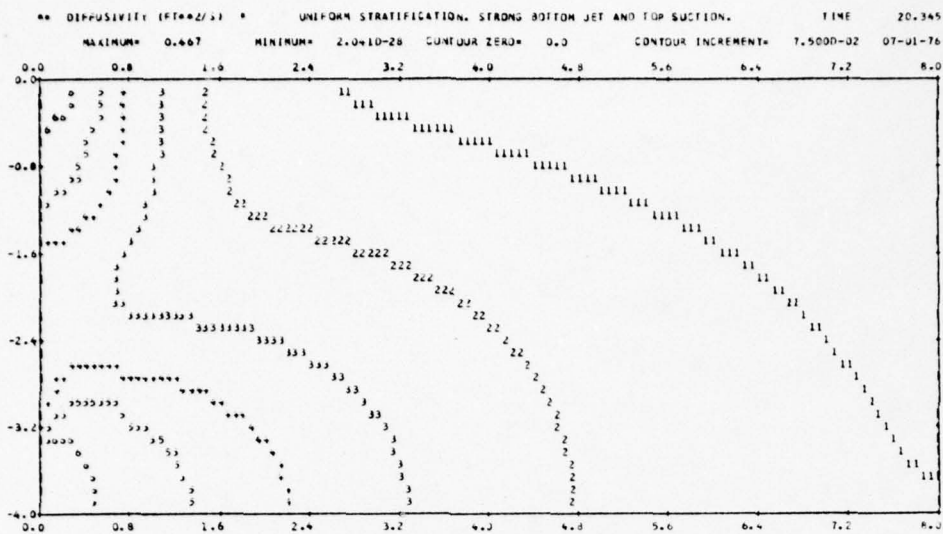


FIGURE 3. Strong Flow Results

FIGURE 4. Strong Flow Results

These results supplement those in Figure 3. The turbulent diffusivity distribution is obtained from a turbulent kinetic energy density equation; it is largest near the left ports, and decreases towards the right-hand boundary. The temperature on the left is barely above 40°F . The flow through the permeable right boundary is much smaller than the imposed flow at the left, because of recirculation.



UNIFORM STRATIFICATION, STRONG BOTTOM JET AND TOP SUCTION.
 4 FOOT DEPTH EXPERIMENT SIMULATION, 1 FOOT JET AND SUCTION.
 BOTTOM JET TEMPERATURE IS 40 DEGREES FAHRENHEIT.
 TEMPERATURE RANGE 40 TO 80 DEGREES AT INFINITY.

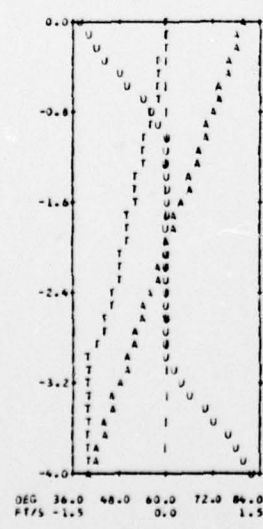
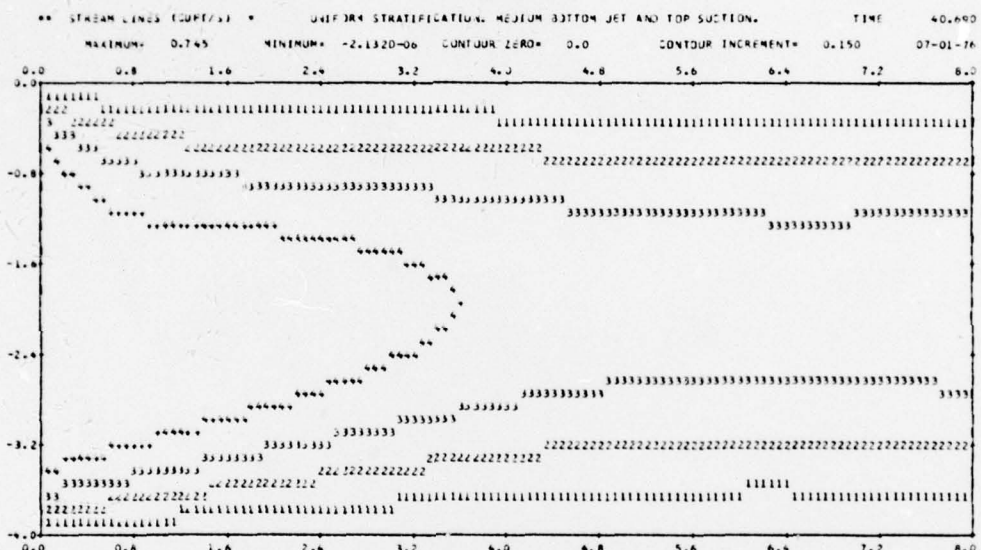
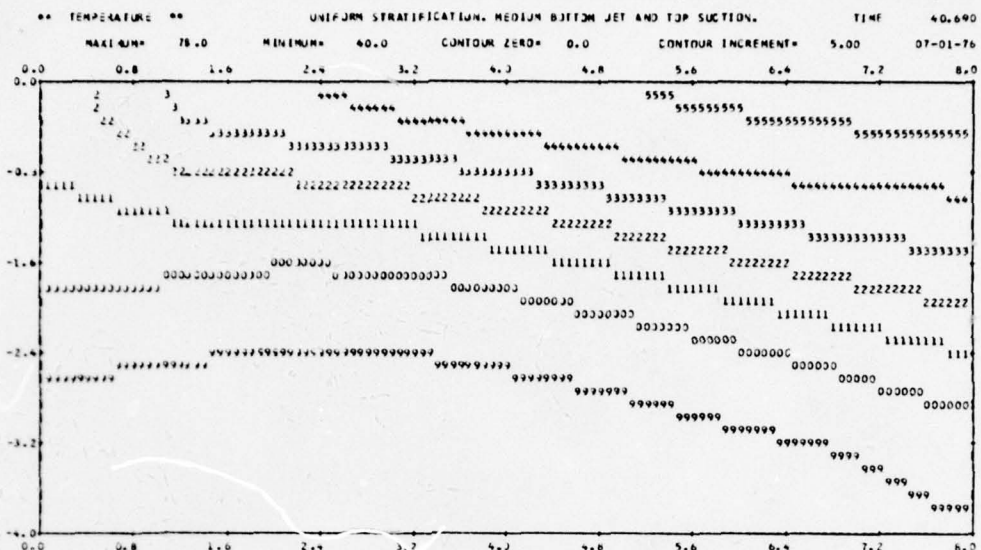
KMPJ 0.8333 -0.4000 0.0 0.0
 LMPJ 0.200 0.200 0.0 0.0
 TANALF 0.0 0.0 0.0 0.0
 TPAHR 40.0 0.0 0.0 0.0
 RPL 0.250 0.250 0.000 0.000
 ZCENT 0.0 1.000 0.0 0.0
 TT,TS,ZT,WID 80.0 40.0 0.700 1000.000
 QANVQJEP 1.00-05 0.50
 TLEN,CFL,C5,CW,PURC 3.100 0.500 0.100 0.500
 GAP,ASTRCH,ISTRCH,II,JJ 2.000 1.700 0.0 12 12
 TIME,CFL,NDUTPT,OSCALE,#TOFT 30.0 0.60 2 4.0 1.0
 07-01-76

MEAN PLANE INFLOW TEMPERATURE IS 49.8

FIGURE 4. Strong Flow Results

FIGURE 5. Medium Flow Results

In the center panel, only one streamline recirculates from the bottom left cold inflow to the top left, while three go out at the right boundary. Three other streamlines bring warm water in at the top right, and leave the region at the top left. The upper panel shows the resulting temperature distribution; the curves 0, 2, and 4 are 50°F , 60°F , and 70°F . Further results are shown in Figure 6.



UNIFORM STRATIFICATION, MEDIUM BOTTOM JET AND TOP SUCTION.

4 FOOT DEPTH EXPERIMENT SIMULATION, 1 FOOT JET AND SUCTION.

BOTTOM JET TEMPERATURE IS 40 DEGREES FAHRENHEIT.

TEMPERATURE RANGE 40 TO 80 DEGREES AT INFINITY.

AMPJ	0.4000	-3.4000	0.0	0.0
AMPQ	0.2000	0.2000	0.0	0.0
TANALP	0.0	0.0	0.0	0.0
TANHR	40.0	0.0	0.0	0.0
AMPL	0.250	0.250	0.000	0.000
ZCENT	0.0	1.000	0.0	0.0
TF,TR,ZTC,WID	80.0	40.0	0.700	1000.000
QANNO3DP		1.00-05	0.50	
TLEN,CF,CS,CG,PDWC	0.100	0.500	0.100	0.500
GAP,ASTACH,ZSTACH,II,JJ	2.000	0.0	0.0	12 12
TIME,CFL,NDUTPT,DISCALE,WIDFT	30.0	0.50	2	4.0 1.0

HEAVY PLANT INFLOW TEMPERATURE IS 56.1

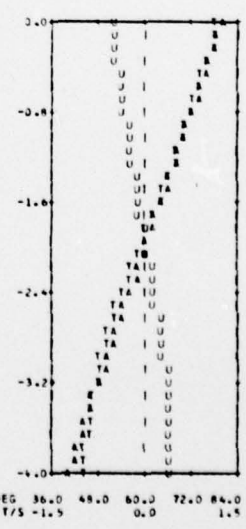
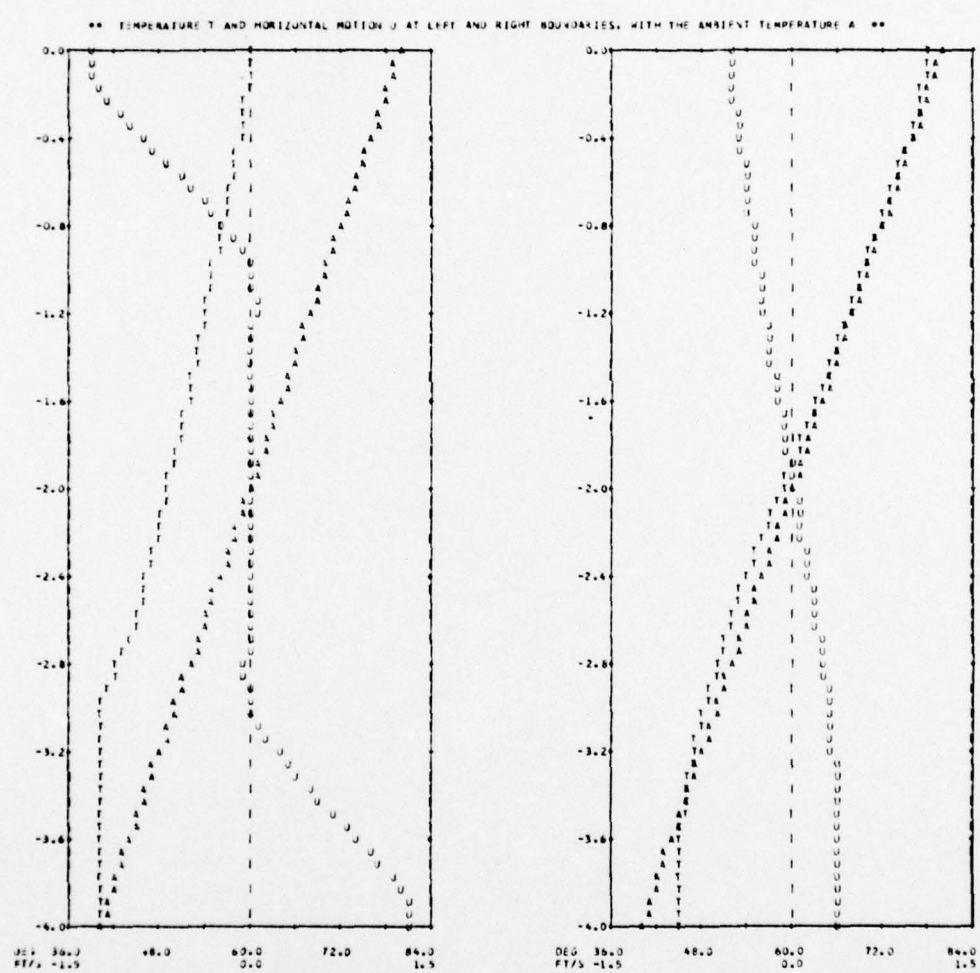
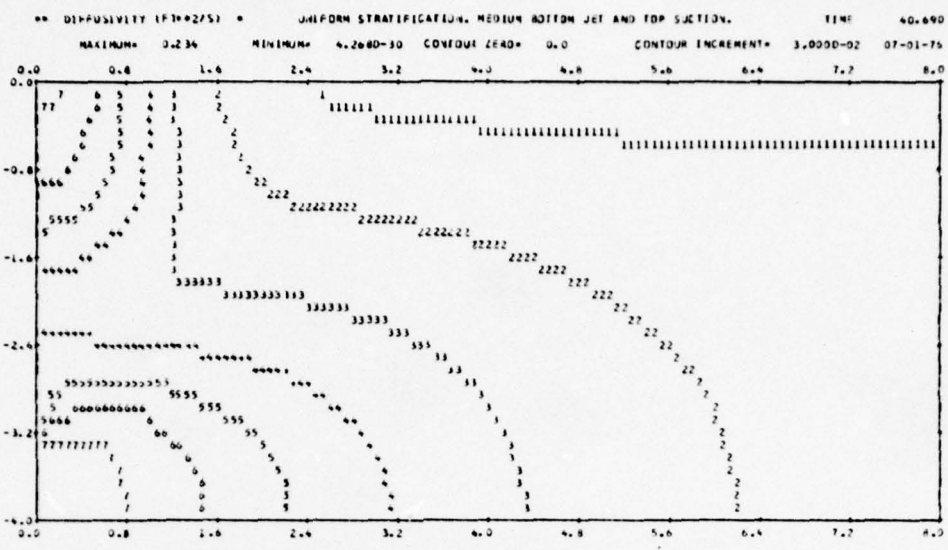


FIGURE 5. Medium Flow Results

FIGURE 6. Medium Flow Results

These results supplement those in Figure 5. The turbulent kinetic energy generated at the left ports is advected by the mean flow, and the derived turbulent diffusivity is, therefore, largest near the ports and in the lower half of the region, as shown in the upper panel. In the center panels, the horizontal fluxes are smaller at the right than at the left, and there is some recirculation. Recirculation and turbulent heat transport make the left temperature much smaller than the ambient stratification.



UNIFORM STRATIFICATION, MEDIUM BOTTOM JET AND TOP SUCTION.

4 FOOT DEPTH EXPERIMENT SIMULATION, 1 FOOT JET AND SUCTION.

SUCTION JET TEMPERATURE IS 40 DEGREES FAHRENHEIT.

TEMPERATURE RANGE 40 TO 80 DEGREES AT INFINITY.

MEAN PLAIN INFLOW TEMPERATURE IS 56.1

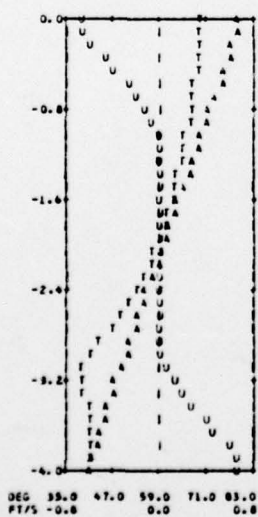
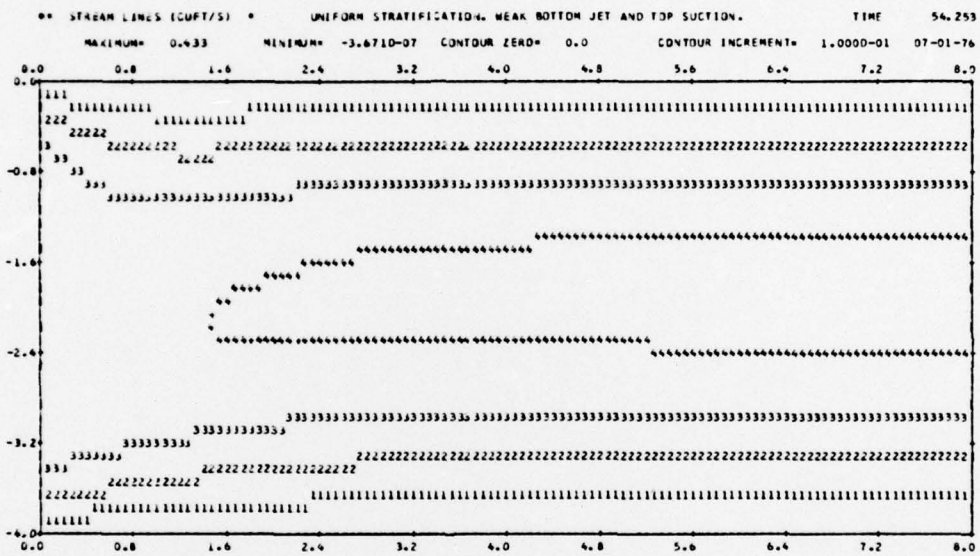
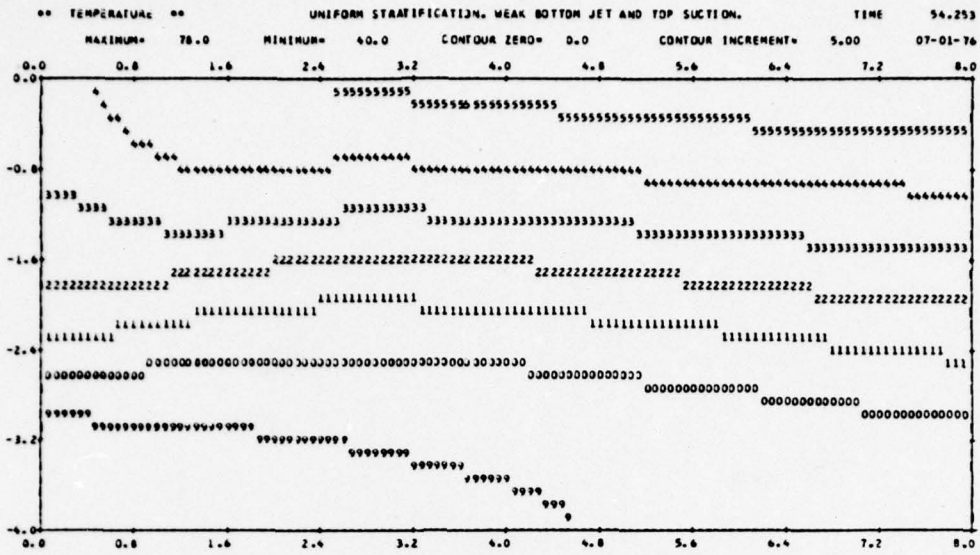
LMPU	0.4300	-0.4000	0.0	0.0
AMPQ	0.200	0.200	0.0	0.0
TANALP	0.0	0.0	0.0	0.0
TEANK	40.0	0.0	0.0	0.0
RPL	0.250	0.250	0.000	0.000
ZCENT	0.0	1.000	0.0	0.0
TT, TB, ZTC, WID	80.0	40.0	0.700	1000.700
QWB, QJEP		1.07-05	0.50	
TLEN, CF, CS, CW, PURC	0.100	0.500	0.100	0.500
GAP, KSTRCH, ZSTRCH, II, JJ	2.000	0.0	0.0	12 12
TIME, CPL, NOUTPT, DSCALE, WIDFT	30.0	0.50	2	4.0 1.0

07-01-76

FIGURE 6. Medium Flow Results

FIGURE 7. Weak Flow Results

In the center panel, the cold turbulent jet at the bottom left entrains an extra streamline and flows out at the right; three streamlines carry warm water from the top right to the top left; and there is no recirculation. The temperature is almost constant on the streamlines, and is little disturbed from the ambient stratification. As shown in the upper panel, there is some turbulent diffusion near the left boundary and in the bottom jet. Further results are shown in Figure 8.



UNIFORM STRATIFICATION, WEAK BOTTOM JET AND TOP SUCTION.
4 FOOT DEPTH EXPERIMENT SIMULATION, 1 FOOT JET AND SUCTION.
BOTTOM JET TEMPERATURE IS 40 DEGREES FAHREHHEIT.
TEMPERATURE RANGE 40 TO 80 DEGREES AT INFINITY.

AMPU	0.2000	-0.2000	0.0	0.0
AMPQ	0.200	0.200	0.0	0.0
TANALP	0.0	0.0	0.0	0.0
TPAHR	40.0	0.0	0.0	0.0
RPL	0.250	0.250	0.000	0.000
ZCENT	0.0	1.000	0.0	0.0
TI, TB, ZTC, WTD	80.0	40.0	0.700	1000.000
QAMB, QDEP	1.00E-05	0.50		
TLEN, CF, CS, CW, PDRC	0.100	0.500	0.100	0.500
GAP, ESTRCH, ESTRCH, II, JJ	2.000	0.0	0.0	12 12
TIME, CR, NOUTPF, DSCALE, WJ, T	20.0	0.80	2	4.0 1.0

MEAN PLANAR INFLOW TEMPERATURE IS 86.8

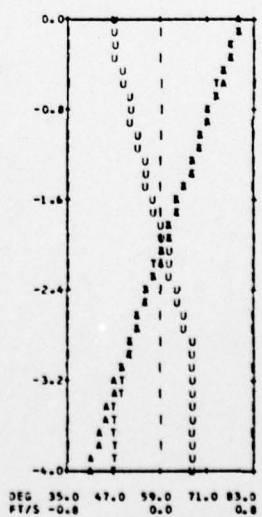


FIGURE 7. Weak Flow Results

FIGURE 8. Weak Flow Results

These results supplement those in Figure 7. The turbulence distribution associated with the bottom jet is almost separate from that near the top left outflow port. The bottom right outflow is larger than the imposed bottom left inflow, because of entrainment. Even on the left boundary, the temperature is not very different from the ambient distribution.

The lower panel of Figures 3 to 8 provides a computer caption, a copy of the input data, the computation date, and the mean temperature of the surface outflow from the region, calculated using equation (17). The three mean temperatures are 49.8°F, 56.1°F, and 66.8°F; the value for strong flow is close to 40°F because most of the surface outflow has come direct from the cold bottom left inflow.

To the left and right of the lower panels in Figures 3, 5, and 7 are plots of \bar{T} and \bar{u} at the left and right boundaries of the computational domain, together with the ambient temperature distribution, all as functions of z . These plots are repeated at double size in the center panel of Figures 4, 6, and 8.

The ambient temperature increases linearly from 40°F to 80°F in each case. The temperature on the left boundary is 40°F in the cold inflow region at the bottom, and increases to temperatures of 52.0°F, 59.6°F, and 69.6°F at the top left boundary. The temperature on the right boundary deviates somewhat from the ambient temperature, but only where the flow is out of the computational domain.

The horizontal flow at the left boundary is given by equation (38), with the three maximum flow speeds U differing by factors of two. The horizontal flow at the right boundary is more than the estimated maximum possible stable flow [cf. equation (36)],

$$\bar{u} = -N(z + 2) \quad , \quad (41)$$

by factors of 1.48, 1.32, and 1.05 in the three cases. The estimate (36) was based on the assumption that \bar{E} is negligibly small near the right boundary; in our three calculations, this was not the case.

The flow (41) corresponds to an outward flux at the bottom right of $0.41 \text{ ft}^2/\text{sec}$, with an equal influx at the top right. The actual fluxes at the right-hand boundary are the stream function maxima on the boundary, respectively, 0.61, 0.54, and $0.43 \text{ ft}^2/\text{sec}$. For the strong and medium flow cases, these fluxes are smaller than the imposed values on the left boundary, and the remaining flux recirculates from the bottom left to the top left.

In all three cases, the bottom left inflow jets entrain some of the surrounding fluid. The total jet flux, including this entrained water, is the stream-function maximum, respectively, 1.45, 0.74, and $0.43 \text{ ft}^2/\text{sec}$ in the three cases.

The turbulent diffusivity $K(x,z)$ is displayed in the upper panel of Figures 4, 6, and 8. The contour increments are 0.075, 0.03, and $0.015 \text{ ft}^2/\text{sec}$. This turbulent diffusivity distribution is the crucial result of the turbulence modelling, since it is the means by which the turbulent kinetic energy density \bar{E} influences the mean flow and temperature. The diffusivity K is largest at the inflow and outflow regions (where it is proportional to U), and decreases away from the left boundary. The minimum value on the left wall is significant, since it determines the momentum and heat transport between the cold lower layers moving to the right and the warm upper layers moving to the left. The three minima are 0.250, 0.115, and $0.043 \text{ ft}^2/\text{sec}$, respectively, and it appears that for still weaker flow the value would become so small that the two flows would be essentially independent.

These numerical results are summarized in Table 1, for purposes of comparison. The left boundary fluxes are proportional to the flow speed U , while the right fluxes are bounded, roughly speaking, by equation (41). The flux difference recirculates from the bottom left inflow to the top left outflow. The bottom turbulent jet entrains some surrounding fluid, which for the non-recirculating weak flow case is drawn in from infinity, with the flow near the surface. The temperature at the top left is smaller than 80°F only because of

TABLE 1. COMPARISON OF NUMERICAL RESULTS FOR THE THREE FLOW CASES

FLOW CASE	STRONG	MEDIUM	WEAK
Maximum Flow Speed U (ft/sec)	2.68	1.34	0.67
Left Boundary Fluxes (ft ² /sec)	1.44	0.72	0.36
Right Boundary Fluxes	0.61	0.54	0.43
Recirculation Flux	0.83	0.18	0.00
Total Entrained Flux	1.45	0.74	0.43
Temperature at Top Left (°F)	52.00	59.60	69.60
Mean Surface Outflow Temperature	49.80	56.10	66.80
Maximum Diffusivity (ft ² /sec)	0.467	0.234	0.117
Minimum Diffusivity on Left	0.250	0.115	0.043

turbulent heat transport; while the mean surface outflow temperature is also reduced by recirculation in the strong and medium flow cases. The diffusivity maxima, and the minima on the left boundary, are also given in the table, for comparison purposes.

In conclusion, we note that for this numerical simulation of our proposed experiment, relatively small increases in the flow speed can produce recirculation, with a substantial reduction in the mean temperature of the warm surface outflow from the experimental tank. The corresponding situation for an OTHF prototype would be a reduction in the temperature difference between the two intakes, resulting in a plant power loss. Further research and experimental verification is required to determine how such a power loss can be avoided.

ACKNOWLEDGEMENTS

This report was prepared as part of the research program, "Theoretical Fluid Dynamical Studies of Resource Availability and Environmental Impact of Ocean Thermal Power Plants", in the Naval Research Laboratory, supported by the Ocean Thermal Energy Conversion Program, Division of Solar Energy, Energy Research and Development Administration, under ERDA contract E (49-26) 1005. The majority of the work was performed under the subcontract N00014-76-C-0610 with Science Applications, Inc.

REFERENCES

1. Dugger, G. L. (1975), "Proceedings, Third Workshop on Ocean Thermal Energy Conversion," Report SR75-2, Applied Physics Lab, Laurel, Md.
2. Trimble, L.C. (1975), "Ocean Thermal Energy Conversion Power Plant Technical and Economic Feasibility," Lockheed Missile and Space Co., Inc., Report NSF/RANN/SE/GI-C937/FR/75/1, Sunnyvale, Calif.
3. Piacsek, S.A., Martin, P.J., Toomre, J., Roberts, G.O. (1976), "Recirculation and Thermocline Perturbations from Ocean Thermal Power Plants," Report NRL-GFD/OTEC 2-76, Geophysical Simulation Section, Code 7750, Naval Research Laboratory, Washington, D.C.
4. Piacsek, S.A., Roberts, G.O. (1975), "Numerical Experiments on Collapsing Submarine Wakes in a Stratified Ocean (U)," Naval Research Laboratory Memorandum Report 3178. CONFIDENTIAL
5. Piacsek, S.A., Toomre, J., Roberts, G.O. (1975), "Geophysical Fluid Dynamics Background for Ocean Thermal Power Plants," Report NRL-GFD/OTEC 11-75, Geophysical Simulation Section, Code 7750, Naval Research Laboratory, Washington, D.C.
6. Douglass, R. (1975), "Ocean Thermal Energy Conversion Research on an Engineering Evaluation and Test Program," Vols 1-5, TRW, Redondo Beach, Calif.
7. Varga, R.S. (1962), "Matrix Iterative Analysis," Prentice-Hall, Englewood Cliffs, N.J.
8. Warn-Varnas, A., Piacsek, S.A. (1976), "Comparison of First and Second Order Turbulence Closure Models," Naval Research Laboratory Memorandum Report, to appear.